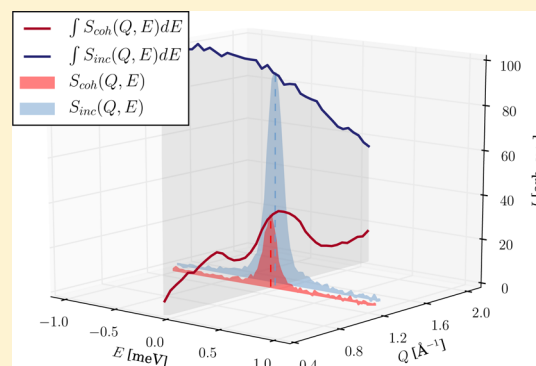


# Collective Ion Diffusion and Localized Single Particle Dynamics in Pyridinium-Based Ionic Liquids

Tatsiana Burankova,<sup>†,‡</sup> Rolf Hempelmann,<sup>†</sup> Andrew Wildes,<sup>¶</sup> and Jan P. Embs<sup>\*,‡</sup><sup>†</sup>Department of Physical Chemistry, Saarland University, Saarbrücken, 66123, Germany<sup>‡</sup>Laboratory for Neutron Scattering and Imaging, Paul Scherrer Institute, Villigen PSI, 5232, Switzerland<sup>¶</sup>Institut Laue-Langevin, Grenoble, 38000, France

**ABSTRACT:** Quasielastic neutron scattering with polarized neutrons allows for an experimental separation of single-particle and collective processes, as contained in the incoherent and coherent scattering contributions. This technique was used to investigate the dynamical processes in the pyridinium-based ionic liquid 1-butylpyridinium bis(trifluoromethylsulfonyl)-imide. We observed two diffusion processes with different time scales. The slower diffusional process was present in both the coherent and the incoherent contribution, meaning that this process has at least a partial collective nature. The second faster localized process is only present in the incoherent scattering contribution. We conclude that it is a true single-particle process on a shorter time scale.



## INTRODUCTION

Quasielastic neutron scattering (QENS) has been demonstrated to be an informative tool for investigating different materials and has been applied to yield comprehensive information about various stochastic processes on a time scale ranging from a fraction of picoseconds to nanoseconds.<sup>1–3</sup> Incoherent neutron spectroscopy is particularly sensitive to hydrogen atoms and can be applied to unravel the dynamics of hydrogen-rich materials. QENS allows one to measure both energy transfer and momentum transfer of scattered neutrons and thus to simultaneously derive information about both time and space characteristics of studied processes. The kinetic energy of cold and thermal neutrons fits excitation energies in condensed matter, the length scales explored in an experiment being comparable with the wavelength of incident neutrons, which is of the order of interatomic distances in solids and liquids. Deuterium labeling is also an asset of QENS for studying separate hydrogen groups of more complex molecules.<sup>4,5</sup>

For a bit more than a decade the above-mentioned advantages of the QENS-technique have been applied in studies on a class of novel materials called ionic liquids (ILs).<sup>5–17</sup> ILs are usually defined as organic salts with melting points below 373 K.<sup>18</sup> Owing to the interplay between different intermolecular interactions (Coulomb, van der Waals), they possess a spectrum of interesting physicochemical properties valuable for different fields.<sup>19,20</sup> For their manifold present and potential applications, especially in electrochemistry,<sup>20</sup> information about their microscopic dynamics is highly demanded. So far the relaxation processes observed in various ILs by different techniques have proved to be decidedly heterogeneous.<sup>21–23</sup> For example, QENS studies on the time scale of several

picoseconds usually point to the existence of two processes: long-range diffusion and motions restricted by the geometry of the cations.<sup>5,10,14,24</sup> The usage of the spectrometer with a finer resolution allows distinguishing further between two diffusional processes, one of which may relate to clustering or nanoscale inhomogeneity effects.<sup>11</sup> However, all these results were obtained under the assumption that the incoherent signal from the hydrogen atoms of the cations determines the total scattering intensity, while the coherent contribution was considered to be negligible. It is a common and quite legitimate approach in analysis of stochastic motions in hydrogen-rich samples. On the other hand, the structure factor of many ionic liquids features some so-called prepeaks in the Q-range accessible normally by QENS.<sup>25–28</sup> Thus, this assumption for such kinds of samples is questionable.

The origin of the prepeaks in ILs is the source of a long-lasting and extensive debate.<sup>26,29</sup> In this respect, the issue has been most thoroughly explored for the class of imidazolium-based ILs. At first, their prepeaks were interpreted as a fingerprint of highly structured domain formation on the nanometer length scale. The presence and position of the first maximum at the lowest Q-value exhibited dependence on both the number of carbon atoms in the side alkyl chains and temperature.<sup>27,30</sup> Therefore, alkyl substitutes were considered as a driving force for this intermediate range order. Owing to recent experiments,<sup>31</sup> this explanation has gained credence. However, the possibility that these low-Q diffraction features reflect nanometer-scale structural organization has been

Received: September 12, 2014

Revised: November 6, 2014

Published: November 11, 2014

questioned. First, the prepeaks or the first sharp diffraction peaks are not a peculiar or exclusive feature of ILs. It was also highlighted that the presence of the bulky alkyl chains leads to different patterns of ion coordination. The prepeaks could be simply a result of this geometrical anisotropy, but not a result of creating complex morphologies from the alkyl tails.<sup>25,29</sup> Thus, the broad peak at around  $1.4 \text{ \AA}^{-1}$  corresponds to the spatial correlation length of  $4.5 \text{ \AA}$  and points to intramolecular and close contact intermolecular interactions (correlations between ion pairs, adjacent alkyl chains). The peak at around  $0.8\text{--}0.9 \text{ \AA}^{-1}$  usually depends on the length of the alkyl chain and is connected with cooperative effects between polar groups of the same sign. In any case, the discussed correlations either in domains on the nanometer length scale or between the nearest neighbors will be reflected in dynamics and in QENS-spectra as a coherent component, which cannot be neglected. To put it differently, both collective dynamics and single-particle dynamics contribute to the broadening of an elastic line, and the analysis of this mixture is not a trivial task.

It is possible to use deuteration or partial deuteration to change the ratio between coherent and incoherent parts.<sup>14,32</sup> Totally deuterated samples are mainly used to study collective relaxation processes by means of neutron spin-echo spectroscopy (NSE).<sup>8,12,16</sup> In contrast to this, works based on the time-of-flight (TOF) measurements focus on single-particle dynamics of protonated or partially deuterated samples.<sup>5,6,9–11,13–15</sup> As studied compounds cannot be usually considered to be purely coherent or incoherent scatterers, the only unambiguous experimental way to circumvent the problem is to make use of polarized neutrons. This fact determined the main objectives of the present work.

After the first successful results on separation of coherent and incoherent scattering of a pyridinium-based IL ([BuPy][Tf<sub>2</sub>N]) obtained on the triple axis spectrometer TASP at the Swiss spallation source (SINQ) and presented in our previous work,<sup>14</sup> we performed this kind of a scattering experiment on the cold neutron diffuse scattering spectrometer D7 at ILL.<sup>33,34</sup> The wide scattering angle simultaneously covered by D7 allowed us to expand the studied range of the wavevector transfer. The aim of the investigation was 2-fold. First, the obtained “pure” incoherent spectra would give access to the values of the time and length characteristics of stochastic processes that are closer to the actual values and would allow an estimation of a systematic error, to which measurements are prone, if one assumes that coherent scattering is negligible and the total scattering is totally incoherent. Second, the coherent contribution was also analyzed, because it is by no means a waste in this kind of experiment. The coherent contribution provides information about dynamical processes of particles with regard to their surroundings.

## EXPERIMENTAL DETAILS

**Sample.** In this study we used a totally protonated sample of 1-butylpyridinium bis(trifluoromethylsulfonyl)imide ([BuPy][Tf<sub>2</sub>N]) (Figure 1). It was characterized and



**Figure 1.** Structure of the studied pyridinium-based ionic liquid

synthesized at the Chemistry Department, Saarland University, as described in our previous publications.<sup>14,17</sup> All the measurements were performed at temperatures above the melting point of ([BuPy][Tf<sub>2</sub>N]) ( $T_m = 24.5 \text{ }^\circ\text{C}^{17}$ ).

Table 1 summarizes the neutron scattering and absorption cross sections for the cation and the anion. We see that the

**Table 1.** Summary of the Neutron Cross Sections of the Studied Species<sup>a</sup>

system	$\sigma_{\text{scatt}}$ (b)	$\sigma_{\text{abs}}$ (b)	$\sigma_{\text{inc}}$ (b)	$\sigma_{\text{coh}}$ (b)	$\sigma_{\text{inc}}/\sigma_{\text{scatt}}$ (%)
[BuPy][Tf <sub>2</sub> N]	1275.58	30.74	1124.81	150.76	88.18
[Tf <sub>2</sub> N]	65.70	9.68	0.52	65.18	0.80
[BuPy]	1209.87	21.07	1124.29	85.59	92.93
–C <sub>4</sub> H <sub>9</sub>	760.51	9.62	722.43	38.06	95.00
–NC <sub>3</sub> H <sub>5</sub>	449.48	11.45	401.85	47.62	89.40

<sup>a</sup> $\sigma_{\text{abs}}$  is given for neutrons with the wavelength of  $5.75 \text{ \AA}$ .  $1 \text{ b} = 10^{-28} \text{ m}^2$ .

incoherent cross section of the [Tf<sub>2</sub>N] anion can be neglected. The coherent scattering from both the cation and the anion are comparable and amount to 12% of the total scattering cross section. To minimize absorption effects, we used an annular hollow cylindrical sample holder made of aluminum. The sample container has the outer diameter of  $14 \text{ mm}$  and the gap between the inner and outer cylinders was  $0.2 \text{ mm}$  guaranteeing that the neutron beam transmission through the sample exceeds 90%. Thus, the effects of multiple scattering are negligible, and unwanted absorption can be considered to be suppressed.

The diffractogram of a totally deuterated sample was measured on the high-resolution powder diffractometer HRPT at SINQ (Figure 2). It features two broad diffraction peaks at  $Q_1 = 0.77 \text{ \AA}^{-1}$  and  $Q_2 = 1.40 \text{ \AA}^{-1}$ , respectively. They correspond to the maxima of the site-site radial distribution functions calculated by Tsuzuki et al. for [BuPy][Tf<sub>2</sub>N] by means of molecular dynamics simulations.<sup>36</sup> The radial distribution function between the nitrogen atoms of the cations

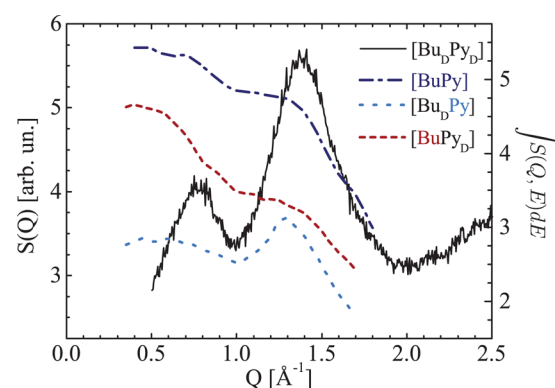


**Figure 2.** Intensity as a function of  $Q$  as measured on a completely deuterated sample, [Bu<sub>D</sub>Py<sub>D</sub>][Tf<sub>2</sub>N] (solid line). The experiment was performed on the thermal neutron diffractometer HRPT at SINQ, using incident neutrons with  $\lambda = 1.5 \text{ \AA}$ . Integrated intensity of the totally protonated sample, [BuPy][Tf<sub>2</sub>N] (dashed–dotted line), and the partially deuterated samples, chain-deuterated, [Bu<sub>D</sub>Py][Tf<sub>2</sub>N] (dotted line), and ring-deuterated, [BuPy<sub>D</sub>][Tf<sub>2</sub>N] (dashed line), was calculated from the QENS-spectra measured on the cold neutron time-of-flight spectrometer FOCUS at SINQ with the wavelength of incident neutrons equal to  $5.75 \text{ \AA}$

exhibits a broad maximum at 7.8 Å; the distribution function between the nitrogen atoms of the [Tf<sub>2</sub>N]<sup>+</sup> anions has a narrower maximum at 8.2 Å. So, the correlation between the charged particles of the same sign contributes to the first diffraction peak Q<sub>1</sub>. The most probable distance between the nitrogen atoms of an adjacent cation and anion equals 5.8 Å. The corresponding wavevector  $Q = 1.1 \text{ Å}^{-1}$  is less than Q<sub>2</sub>, but, as discussed in the Introduction, not only correlations between ion pairs may contribute to the second diffraction maximum. Therefore, exact agreement between the values cannot be expected. The diffraction spectrum can be compared with the integrated intensities obtained in our previous QENS-experiments<sup>5</sup> on the protonated and partially deuterated samples as well (Figure 2). The integrated intensity is calculated by integration of the dynamic structure factor only within a limited instrumental energy window and, hence, cannot be considered to be the pure static structure factor. Nevertheless, the comparison between these quantities is justified. Thus, the deuteration of the butyl-chain intensifies the peak at  $Q = 1.3 \text{ Å}^{-1}$ . This indicates that this structural maximum is linked to the correlations between the alkyl substituents.

**D7 Experiment.** The diffuse scattering spectrometer D7 at ILL<sup>33,34</sup> has the option of polarizing the incident beam and is equipped with supermirror analyzer detector banks covering a 132° angular range, allowing uniaxial polarization analysis used for separation of coherent and spin-incoherent scattering in nonmagnetic samples. A magnetic guide field of about 10–20 G is maintained along the path of the incident and scattered neutrons everywhere within D7 to preserve the spin-state of the neutron. For our experiments we set the wavelength to 4.86 Å. The addition of a Fermi chopper allowed us to take advantage of the time-of-flight-mode with the neutron polarization perpendicular to the scattering plane and, thus, to measure the change in the direction and energy of the scattered neutrons, as well as the change in the spin state simultaneously. The efficiency of the detectors was calibrated by measuring a vanadium standard. The vanadium spectra were also used as the resolution function  $R(Q, E)$  of the instrument, the corresponding energy resolution (fwhm) being equal to 140 μeV. For the selected wavelength of incident neutrons the dynamic range amounted to ± 2 meV, the wavevector transfer covering the region of 0.6–2.2 Å<sup>−1</sup>. Empty can runs and sample transmission measurements were performed to subtract corresponding background contributions.

As it follows from the theoretical principles of the polarization analysis,<sup>33,37</sup> the total single scattering intensities without ( $I_{\uparrow\uparrow}$ , nonspin-flip intensity) and with ( $I_{\uparrow\downarrow}$ , spin-flip intensity) the change in the neutron-spin state are given by

$$I_{\uparrow\uparrow} = I_{\text{coh}} + \frac{1}{3}I_{\text{inc}} \quad (1a)$$

$$I_{\uparrow\downarrow} = \frac{2}{3}I_{\text{inc}} \quad (1b)$$

where  $I_{\text{coh}}$  and  $I_{\text{inc}}$  are the intensities of coherent and incoherent scattering, respectively. Equations 1a and 1b are only valid in the ideal case; in practice the properties of the measuring equipment and its imperfections should be taken into consideration. The quality of the instrument is characterized by the so-called “flipping ratio”, measured in an additional run for each detector with a quartz standard, which is a purely nonspin flip scatterer. The mean value of  $R$  was equal to 10. Therefore, detectors with the  $R$ -value less than five were

excluded from the subsequent data reduction process ( $R$ -values below five mostly emerged at high  $2\theta$ -values), resulting in the reduction of the theoretically possible  $Q$ -space, accessible for analysis.

The corrected nonspin flip and spin flip intensities read as<sup>38</sup>

$$I_{\text{corr}}^{\uparrow\uparrow} = I^{\uparrow\uparrow} + \frac{1}{R-1}[I^{\uparrow\uparrow} - I^{\uparrow\downarrow}] \quad (2a)$$

$$I_{\text{corr}}^{\uparrow\downarrow} = I^{\uparrow\downarrow} - \frac{1}{R-1}[I^{\uparrow\uparrow} - I^{\uparrow\downarrow}] \quad (2b)$$

and the final expressions for the coherent and spin-incoherent scattering intensities are given as

$$I_{\text{coh}} = I_{\text{corr}}^{\uparrow\uparrow} - \frac{1}{2}I_{\text{corr}}^{\uparrow\downarrow} \quad (3a)$$

$$I_{\text{inc}} = \frac{3}{2}I_{\text{corr}}^{\uparrow\downarrow} \quad (3b)$$

**Data Analysis.** We used the LAMP<sup>39</sup> and DAVE<sup>40</sup> software packages for the data reduction and the analysis of separate  $Q$ -groups. The simultaneous analysis of 2D-scattering maps  $S(Q, E)$  was carried out directly in the IDL-environment (<http://www.exelisvis.com/ProductsServices/IDL/Language.aspx>) using the MPfit procedure.<sup>41</sup> A fitting routine with the two independent variables,  $Q$  and  $E$ , is beneficial and produces more consistent and stable results for complex models with a rather large number of adjustable parameters.

In what concerns the single-particle dynamics and the incoherent scattering, we used a two-step approach for the analysis of our data. The first step is a model-independent analysis, which allows us to estimate the number of processes distinguishable on the time-scale accessible by the spectrometer used and to qualitatively judge the characteristics of stochastic motions. On the time-scale of several picoseconds, two dynamical processes are usually observed.<sup>6,10,14</sup> The slower one is spatially unrestricted and related to the self-diffusion of the cations. The rotation of the cations as a whole is slow<sup>42</sup> and also contributes to the QENS broadening associated with the slow process. The faster dynamics are localized and connected to such motions as out-of-plane libration of the aromatic ring, conformational changes of the butyl-chain, and chain libration. Thus, for ILs the incoherent dynamic structure factor in the quasielastic region can be given as a convolution of the global and localized dynamic structure factors multiplied by the Debye–Waller factor:

$$S_{\text{inc}}(Q, E) = \exp(-2W)S_{\text{glob}}(Q, E) \otimes S_{\text{loc}}(Q, E) \quad (4)$$

In the model-independent approach the global and localized dynamics can each be presented by a Lorentzian function:

$$S_{\text{glob}}(Q, E) = \frac{1}{\pi} \frac{\Gamma_{\text{glob}}(Q)}{\Gamma_{\text{glob}}^2(Q) + E^2} \quad (5)$$

$$S_{\text{loc}}(Q, E) = \text{EISF}(Q)\delta(E) + [1 - \text{EISF}(Q)] \frac{1}{\pi} \frac{\Gamma_{\text{loc}}(Q)}{\Gamma_{\text{loc}}^2(Q) + E^2} \quad (6)$$

The two linewidths  $\Gamma_{\text{glob}}$  and  $\Gamma_{\text{loc}}$  describe the broadening in the energy domain caused by the global and local dynamic processes, respectively.  $\text{EISF}(Q)$  in eq 6 represents the elastic incoherent structure factor<sup>43</sup> of the localized motion and



provides insight into the geometry of the spatial confinement, in which the localized process occurs.

The simplest form of the incoherent dynamic structure factor (eq 4–6) has been successfully applied to a number of complex systems<sup>44–46</sup> and can be considered being a good starting point for the interpretation of QENS data on ILs. For a more comprehensive analysis explicit analytical expressions or models for  $S_{\text{loc}}(Q, E)$  and  $S_{\text{glob}}(Q, E)$  are required. In this work we used the jump-diffusion model<sup>47</sup> proposed by Singwi and Sjölander to describe the unrestricted translational motion. In this case  $\Gamma_{\text{glob}}(Q)$  in eq 5 reads

$$\Gamma_{\text{glob}}(Q) = \frac{\hbar D Q^2}{1 + D Q^2 \tau_0} \quad (7)$$

where  $D$  is the diffusion coefficient and  $\tau_0$  is the residence time between two successive jumps. The model denoted below as the Gaussian model<sup>48,49</sup> was applied to describe the localized dynamics of the particles in the confinement with a “soft” boundary:

$$S_G(Q, E) = e^{-Q^2 \sigma^2} \times \left[ \delta(E) + \sum_{n=1}^{\infty} \frac{(Q^2 \sigma^2)^n}{n!} \frac{1}{\pi} \frac{\hbar n D_{\text{loc}} / \sigma^2}{(\hbar n D_{\text{loc}} / \sigma^2)^2 + E^2} \right] \quad (8)$$

where  $D_{\text{loc}}$  denotes the diffusion coefficient of the localized motion and  $\sigma$  characterizes the size of the domain, in which the particles are diffusing. The coherent contribution can be analyzed using the model-independent approach as well. However, in contrast to the incoherent scattering, the major problem in applying the further steps is the lack of analytical models, which describe coherent QENS,<sup>50,51</sup> especially in the case of localized motions.<sup>52</sup> Although the coherent contribution is a source of valuable information, because it provides insight into collective processes and interference effects, the works on coherent quasielastic scattering are sparse. In comparison with monatomic liquids<sup>53</sup> or with light interstitials in metal lattices<sup>54</sup> the picture of ion motions is complicated by localized processes in addition to the long-range diffusion. Still, some common approaches such as Vineyard's approximation<sup>55</sup> and Sköld's ansatz<sup>50,53</sup> can be applied as a first step to analyze the data.

Vineyard studied the relationship between the coherent and incoherent quasielastic component in the so-called static approximation.<sup>55</sup> He started with the assumption that the time-displaced pair distribution function (van Hove correlation functions) can be expressed by the self-part of this function and the radial-distribution function  $g(\mathbf{r}')$ :

$$G(\mathbf{r}, t) \cong G_s(\mathbf{r}, t) + \int g(\mathbf{r}') G_s(\mathbf{r} - \mathbf{r}', t) d\mathbf{r}' \quad (9)$$

Vineyard's ansatz results in the following simple relation between  $S_{\text{coh}}(Q, E)$  and  $S_{\text{inc}}(Q, E)$ :

$$S_{\text{coh}}(Q, E) = S_{\text{inc}}(Q, E) S(Q) \quad (10)$$

where  $S(Q)$  is the static structure factor. However, eq 10 does not fulfill the second moment sum rule.<sup>56</sup> The ad-hoc substitution of  $Q$  by  $Q/(S(Q))^{1/2}$  introduced by Sköld<sup>50,53</sup> overcomes this problem:

$$S_{\text{coh}}(Q, E) = S_{\text{inc}}\left(\frac{Q}{\sqrt{S(Q)}}, E\right) S(Q) \quad (11)$$

The same result was obtained by Leitner and Vogl<sup>57</sup> considering the diffusion of interacting particles on a Bravais lattice in the limit of weak or short-order interactions. Qualitatively Sköld's approach may be understood in the following way.<sup>50</sup> The coherent intensity is composed of the scattering from several atoms,  $S(Q)$  being the measure of the effective number of atoms which contribute to the intensity at wave vector  $Q$ . The recoil energy transferred to the system is therefore  $S(Q)$  times less, the same as if the recoiling mass were  $S(Q)$  times greater. The coherent dynamic structure factor applied to the analysis of the coherent contribution was based on eq 10 and eq 11; its explicit analytical form will be discussed in the next section.

Finally, correction for resolution distortion has to be undertaken for both the coherent and incoherent contributions. The following form of the scattering law, which contains a convolution operation with the resolution function, should be used to fit experimental spectra accordingly:

$$S_I(Q, E) = I_0(Q) \cdot [S(Q, E) \otimes R(Q, E)] + a + bE \quad (12)$$

$I_0(Q)$  includes an intensity factor and the Debye–Waller factor; the term  $a + bE$  represents a linear background, which accounts for processes faster than the instrument range and  $R(Q, E)$  represents the resolution function of the instrument.

## RESULTS AND DISCUSSION

**Incoherent Contribution.** Following the method described in the experimental section, the coherent and spin-incoherent contributions of the total scattering from the [BuPy][Tf<sub>2</sub>N] sample at four different temperatures were separated. The 2D-intensity maps at  $T = 300$  K are presented in Figure 3. Figure 4a shows the integrated intensities as a function of  $Q$ , and in Figure 4b we present constant  $Q$ -cuts along  $Q = 1.3 \text{ \AA}^{-1}$ . From the integrated intensities we see that the incoherent component decreases gradually with the wavevector transfer in accordance with energy redistribution due to the high frequency vibrations (Debye–Waller factor). The coherent integrated intensity follows the structure factor measured on the totally deuterated sample (Figure 2). Figure 4b demonstrates the spectra at  $Q = 1.3 \text{ \AA}^{-1}$ . Though the incoherent signal dominates in the QENS spectra of the studied IL as in those of other hydrogen-rich materials, Figure 4 clearly shows that the intensity from coherently scattered neutrons cannot be ignored. This is even more important for  $Q$ -values around  $1.3 \text{ \AA}^{-1}$  where correlations between the nearest neighboring particles show up in the diffraction spectrum (see Introduction).

Once the coherent and spin-incoherent contributions had been separated, the comparative analysis of both the incoherent and total spectra were performed. The aim was to explore how the presence of coherent scattering influences the numerical values of the time and length characteristics of the studied processes. At first, a model independent fit was applied. Both the total spectra and the incoherent spectra are satisfactorily described as a superposition of two Lorentzian curves (eq 4–6). In other words, no elastic contribution is present, and two different processes can be resolved on the time scale of the experiment.

The line width  $\Gamma_{\text{glob}}(Q)$  of the narrower Lorentzian contribution tends to 0 at small  $Q$ -values (Figure 5a) in the same way as for long-range diffusional processes (eq 7). The linewidths of the incoherent contribution were found to be

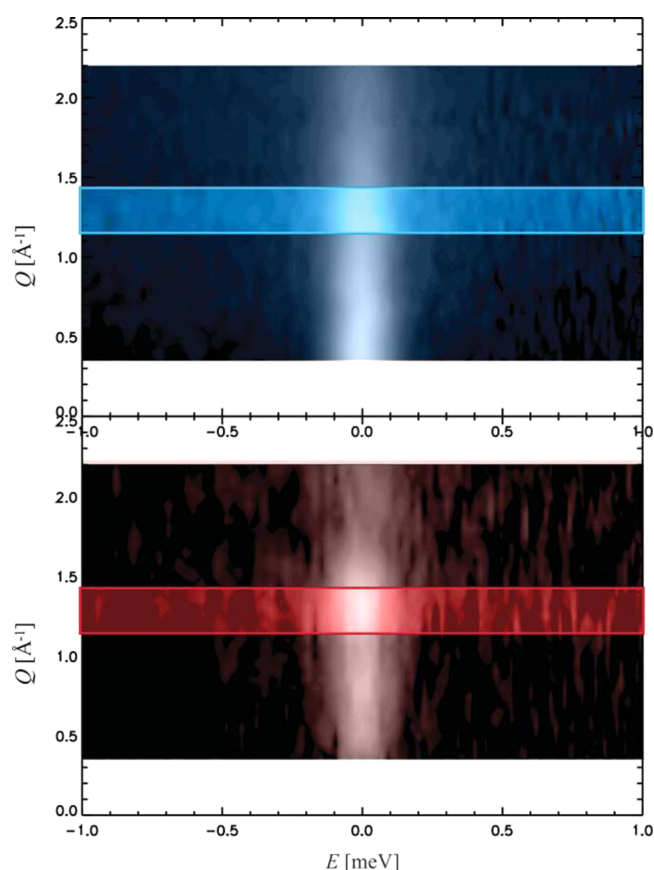


**Figure 3.** Intensity maps of the incoherent (upper panel) and coherent (lower panel) contributions of [BuPy][Tf<sub>2</sub>N] at  $T = 300$  K. Data shown are interpolated to constant  $Q$ -values.

prone to larger values than those of the total spectra. If the input spectra are not corrected for the coherent scattering, the corresponding function has even a kind of modulation following the structure factor; the line width  $\Gamma_{\text{glob}}(Q)$  is clearly narrower than that of the incoherent spectra at  $Q = 1.3 \text{ \AA}^{-1}$ . These modulations are even more pronounced for the totally deuterated sample studied in the recent work,<sup>14</sup> when the coherent scattering dominates. This phenomenon, often referred to as “de Gennes narrowing”, may be considered as a structural relaxation with longer lifetimes and was observed for some other systems.<sup>53,58</sup> The line width  $\Gamma_{\text{loc}}(Q)$  of the broader Lorentzian contribution tends to an almost constant nonzero value at small  $Q$ -values (Figure 5b), thus giving an indication of a movement in a confined region. As well as in the case of the totally deuterated sample studied before, the presence of the intense coherent scattering around  $Q = 1.3 \text{ \AA}^{-1}$  is not reflected in the line width of the spatially restricted dynamics for both the total spectra and the purely incoherent contribution. On the other hand, the separation of the components led to broadening of  $\Gamma_{\text{loc}}(Q)$  of the purely incoherent part of the spectra.

As the diffusion coefficients of the unrestricted and localized motions,  $D$  and  $D_{\text{loc}}$ , are evaluated from the  $\Gamma_{\text{glob}}(Q)$  and  $\Gamma_{\text{loc}}(Q)$  dependencies (see eq 7 and eq 8), it means that a systematic error will be encountered in estimated time characteristics. If the coherent scattering is not taken into account, the diffusion coefficients tend to lower values than the actual ones. On the other hand, the EISF, which contains the information about the geometry of the localized motion, turned

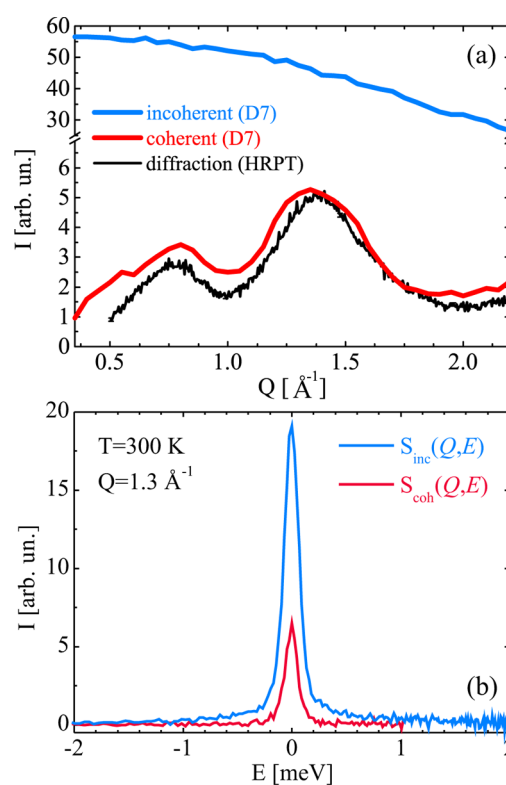


**Figure 4.** (a) Integrated intensity over the energy range of  $[-2.0; 2.0]$  meV as a function of  $Q$ . (b) Constant  $Q$ -cuts taken through the measured spectra  $S(Q, E)$  of the incoherent and coherent components at  $Q = 1.3 \text{ \AA}^{-1}$ .

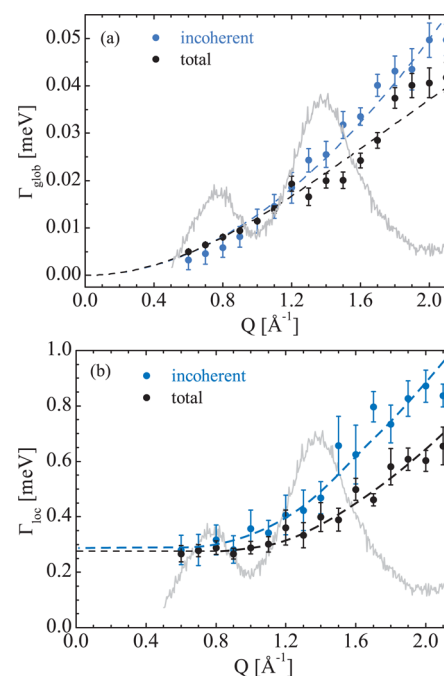


**Figure 5.**  $Q$ -dependencies of the line width characterizing the global (a) and localized (b) dynamics of [BuPy][Tf<sub>2</sub>N] and evaluated from the incoherent part of the spectrum as well as from the total spectrum at  $T = 300$  K. The gray solid line is the diffraction spectrum measured on the completely deuterated sample.

out to be almost identical for the total spectra and the purely incoherent spectra. It means that spatial parameters of the

system may be estimated quite well only from spectra with unseparated components.

For the analysis of the incoherent spectra the jump-diffusion model (eq 7) for the long-range process and the Gaussian model (eq 8) with one radius of confinement for the localized dynamics were employed:

$$S_{\text{inc}}(Q, E) = I_{\text{inc}}(Q) \cdot \frac{1}{\pi} \frac{\Gamma_{\text{glob}}}{\Gamma_{\text{glob}}^2 + E^2} \otimes S_{\text{G}}(Q, E; D_{\text{loc}}) \otimes R(Q, E) + a + bE \quad (13)$$

where  $I_{\text{inc}}(Q) = I_0^{\text{inc}} \exp(-2W(Q))$  is the intensity factor of the incoherent contribution. It gradually decreases with  $Q$  in the same way as the integrated intensity presented in Figure 4a.

In our previous study on partially deuterated samples of [BuPy][Tf<sub>2</sub>N]<sup>5,17</sup> we had to use a distribution function of radii in the dynamic structure factor to model the flexibility of the alkyl chain and to describe the variety of possible localized motions of both the chain and the ring. The fact that only one characteristic size is necessary to capture the broader quasielastic contribution in the present work is explained by a coarser resolution function of the D7 spectrometer (fwhm = 140  $\mu\text{eV}$ ) than that of FOCUS ( $\lambda = 5.75$  Å, fwhm = 60  $\mu\text{eV}$ ) used before and, hence, by a shorter observation time. The radii of confinement and the other parameters of eq 13 evaluated at different temperatures are presented in Table 2.

**Table 2. Diffusion Coefficients of the Global,  $D$ , and Localized Motion,  $D_{\text{loc}}$ , Characteristic Radii of Confinement  $\sigma$  and Residence Time  $\tau_0$  as Obtained from the Incoherent Spectra of the [BuPy] Sample with Equation 13 at Different Temperatures**

$T$ , K	$D \cdot 10^{-10}$ , $\text{m}^2/\text{s}$	$\tau_0$ , ps	$D_{\text{loc}} \cdot 10^{-10}$ , $\text{m}^2/\text{s}$	$\sigma$ , Å
300.0	$2.44 \pm 0.03$	$7.3 \pm 0.4$	$9.34 \pm 0.05$	$0.416 \pm 0.003$
320.0	$3.21 \pm 0.04$	$5.9 \pm 0.3$	$10.7 \pm 0.07$	$0.492 \pm 0.003$
340.0	$4.73 \pm 0.04$	$5.7 \pm 0.3$	$14.1 \pm 0.07$	$0.567 \pm 0.003$
360.0	$5.51 \pm 0.04$	$4.6 \pm 0.3$	$15.7 \pm 0.08$	$0.636 \pm 0.004$

The diffusion coefficients of the long-range motion and the localized motion differ by a factor of 3–5 and their temperature dependence is consistent with the Arrhenius law (Figure 7). The activation energy values equal 12.3 and 8.2 kJ/mol for the global and local processes, respectively, and are in agreement with the values calculated from the FOCUS spectra.<sup>17</sup> The values of  $D_{\text{loc}}$  obtained in the present and previous experiments are also fairly similar within the experimental error. However, the diffusion coefficients of the long-range motion calculated from the D7 data are systematically larger than those of FOCUS. There are three factors that can explain this difference. First, the extraction of the purely incoherent spectra leads to larger values of the linewidths and, consequently, of the diffusion coefficients as it was shown before. Second, owing to the heterogeneous dynamics in ILs, the values of the time characteristics can be influenced by the line width of the instrumental resolution function. This effect was observed for other systems as well.<sup>44</sup> Finally, the resolution available for the D7 experiments was about three times larger than the resolution of FOCUS, and thus the values of the diffusion coefficients obtained from the D7 data differ from those measured on FOCUS.

The same calculations were performed for the spectra with the unseparated contributions. The difference in the equivalent

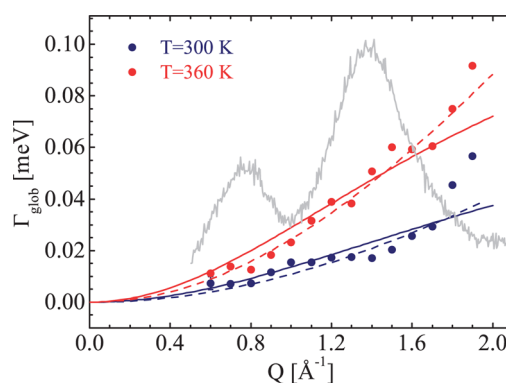
values of the diffusion coefficients amounts to 10–20%, of the radii,  $\sim 1\%$ . So, as already discussed above, the coherent contribution affects time characteristics first of all and, in this respect, should not be neglected.

**Coherent Contribution.** As it can be expected from eq 10 and eq 11, the coherent contribution might be a kind of a “copy” of the incoherent component with the modulated intensity and the linewidths. However, it turned out that the coherent part of the spectra can be presented by a single Lorentzian. The linewidths of the Lorentzian curves are close to the values obtained for the long-range diffusion from the incoherent contribution. The  $Q$ -dependence of this broadening also tends to zero at small  $Q$ -values like for other long-range motions. Therefore, for the further data evaluation the following function based on Vineyard’s approximation was used in the fitting routine:

$$S_{\text{coh}}(Q, E) = I_0^{\text{coh}}(Q) \cdot \frac{1}{\pi} \frac{\Gamma_{\text{glob}}}{\Gamma_{\text{glob}}^2 + E^2} \otimes R(Q, E) + a + bE \quad (14)$$

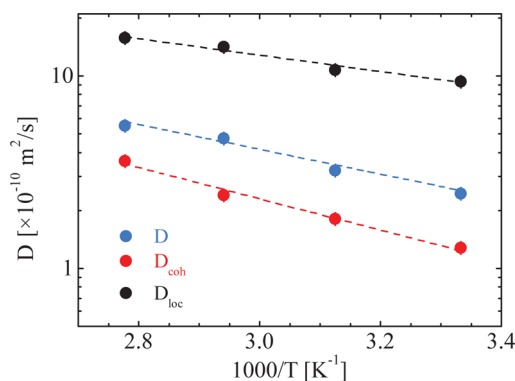
where  $\Gamma_{\text{glob}}$  is expressed by eq 7 in terms of the jump diffusion model and  $I_0^{\text{coh}}(Q)$  is the intensity factor of the coherent contribution. Otherwise stated, we assumed only a diffusional process relevant for the coherent component. The localized dynamics were not considered, because the second Lorentzian curve was not necessary to capture the profile of the spectra.

Figure 6 shows two  $Q$ -dependencies of the Lorentzian line width at two different temperatures with the function (eq 7),



**Figure 6.**  $Q$ -dependence of the coherent quasielastic broadening at different temperatures. The dashed lines are the fits of the coherent component according to eq 14; the solid lines are fits of the incoherent component according to eq 13. The gray solid line is the diffraction spectrum measured on the completely deuterated sample.

which fits to the experimental points quite well. The shortcoming of this approach, however, is that the diffusion coefficients are different from those obtained from the incoherent contribution (Figure 7) and the modulation of the line width is still observed at the  $Q$ -values corresponding to the maxima of the static structure factor. The difference between the values of the diffusion coefficients could be explained, first, by the fact that the source of the coherent scattering is not only the cation but the anion as well. Second, in contrast to incoherent QENS, which gives access to the self-diffusion coefficient, coherent QENS yields the  $Q$ -dependent collective diffusion coefficient, which tends to the bulk diffusion coefficient in the macroscopic limit ( $Q \rightarrow 0$ ).<sup>1</sup> The self-



**Figure 7.** Arrhenius' plots of the diffusion coefficients characterizing the long-range,  $D_{\text{coh}}$  and  $D$ , and spatially restricted diffusion,  $D_{\text{loc}}$ .

diffusion coefficient is connected with spontaneous mixing of particles in thermodynamic equilibrium, whereas the bulk diffusion coefficient is related to the relaxation time of long-range density fluctuations. Nevertheless, the modulation of the linewidths remains a problem for this approach (eq 14). Vineyard's approximation does not explain "de Gennes narrowing" and, therefore, was criticized.

To apply Sköld's ansatz, the static structure factor of the sample is needed. Unfortunately, the actual static structure factor of the studied IL is not available. However, the intensity factor  $I_0^{\text{coh}}(Q)$  is definitely connected with this characteristic and, in the first approximation, may be considered to be proportional to  $S(Q)$  and to the Debye–Waller factor,  $\exp(-2W(Q))$ . The  $Q$ -dependence of the latter can be estimated from the incoherent contribution, so that only one additional parameter, the proportionality constant  $\alpha$ , is required for the fit model. If to assume that  $I_0^{\text{coh}}(Q) = \alpha S(Q) \exp(-2W(Q))$ , the dynamic structure factor reads:

$$S_{\text{coh}}(Q, E) = I_0^{\text{coh}}(Q) \cdot \frac{1}{\pi} \frac{\Gamma'_{\text{glob}}}{\Gamma'^2_{\text{glob}} + E^2} \otimes R(Q, E) + a + bE \quad (15)$$

where  $\Gamma'_{\text{glob}}$  is the line width of the diffusional process modified according to eq 11:

$$\Gamma'_{\text{glob}}(Q) = \frac{\hbar D_{\text{coh}} Q^2 \frac{\alpha \exp(-2W(Q))}{I_0^{\text{coh}}(Q)}}{1 + D_{\text{coh}} Q^2 \frac{\alpha \exp(-2W(Q))}{I_0^{\text{coh}}(Q)} \tau_0} \quad (16)$$

The fitting routine with eq 15 and eq 16 was carried out at temperature  $T = 300$  K, because quite a noisy signal at elevated temperatures rendered the procedure unstable. The estimated value of  $\alpha = 6.3 \pm 0.2$  and the intensity factor as a function of  $Q$  are shown in Figure 8. At the same time the diffusion coefficient reached the corresponding value of the incoherent contribution. Unfortunately, the absence of reliable results at the other temperatures (one of the parameters has to be fixed in the fitting routine) does not allow us to completely approve the validity of this approach for ILs. Nevertheless, the simple (and theoretically not supported) ad hoc modification (eq 11) captures the modulations of the line width and decreases the difference between the diffusion coefficients obtained from the coherent and incoherent parts.

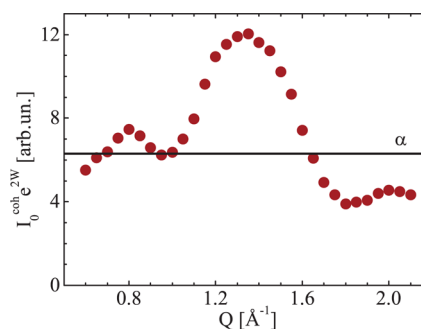


**Figure 8.** Intensity factor  $I_0^{\text{coh}} \exp(2W)$  and  $\alpha$  derived for the coherent component of the spectrum at  $T = 300$  K according to eq 15 and eq 16.

## CONCLUSIONS

Experimental separation of coherent and spin-incoherent scattering, which gives insight into collective and single-particle dynamics, respectively, has been performed for the pyridinium-based IL  $[\text{BuPy}][\text{Tf}_2\text{N}]$  on a picosecond time-scale using the time-of-flight technique with the polarization analysis. Two processes were observed in the incoherent contribution of the QENS spectra. The first slower process is diffusive in nature, the line width of this process can be well described by the jump-diffusion model. The faster dynamics are spatially restricted and determined by various motions like out-of-plane libration of the pyridinium-ring, libration of the butyl-chain, and conformational changes in the skeleton of the alkyl substituent. The localized process is not affected by the structure of the IL, it appears only in the incoherent QENS-spectra. Therefore, the localized dynamics can be considered to be true single-particle processes in nature.

The diffusional process, on the contrary, shows up both in the coherent and incoherent contributions. At those  $Q$ -values, where there are the maxima of the static structure factor, the modulation of the line width of the narrow Lorentzian curve is observed. Indeed, the maxima of  $S(Q)$  indicate that the particles prefer to build local arrangements, in which the energetically favored correlated motion of the neighboring particles slows down the diffusion. It takes more energy to disassemble such arrangements and hence they are longer-lived, and the narrowing of the Lorentzian line width is detected. For example, the structural maximum at  $Q = 1.3 \text{ \AA}^{-1}$  can be intensified by applying partial deuteration of the alkyl substituent. This shows that the coherence in the diffusive motion of neighboring cations may occur through interaction of adjacent butyl-chains. On the basis of these findings, we may conclude that the long-range process has at least a partial collective nature.

QENS experiments with the polarization analysis are very promising in the case of partially deuterated samples as well. Allowing for the investigation of distinct groups of hydrogen atoms, partial deuteration of the samples leads to the more intense coherent contribution at the same time. Then, on one hand, separation of the coherent and spin-incoherent components would provide means to study the pure single-particle dynamics of the separate groups of the cation, and on the other hand, it would allow the acquisition of spectra of the coherent dynamic structure factor, characterized by better statistics in the case of deuterated samples. In general, a more systematic QENS study with polarized neutrons is required for the future.



## AUTHOR INFORMATION

### Corresponding Author

\*E-mail: jan.embs@psi.ch.

### Notes

The authors declare no competing financial interest.

## ACKNOWLEDGMENTS

Financial support by the German Research Foundation (DFG) within the Scientific Priority Program SPP 1191 Ionic Liquids, is gratefully acknowledged (Project No. HE2403/8-3). The authors acknowledge the Institute Laue-Langevin (ILL) for beam time on the diffuse scattering spectrometer D7. We would like to thank V. Fossog for synthesizing the samples and Dr. G. Nilsen for his support during our experiments at D7 and fruitful discussion.

## REFERENCES

- Hempelmann, R. *Quasielastic Neutron Scattering and Solid State Diffusion*; Oxford Series on Neutron Scattering in Condensed Matter; Clarendon Press: Oxford, 2000.
- Fitter, J.; Gutberlet, T.; Katsaras, J., Eds. *Neutron Scattering in Biology*; Biological and Medical Physics, Biomedical Engineering; Springer: New York, 2006.
- Sakai, V. G.; Arbe, A. *Curr. Opin. Colloid Interface Sci.* **2009**, *14*, 381–390.
- Genix, A.; Arbe, A.; Colmenero, J.; Wuttke, J.; Richter, D. *Macromolecules* **2012**, *45*, 2522–2536.
- Embs, J. P.; Burankova, T.; Reichert, E.; Fossog, V.; Hempelmann, R. *J. Phys. Soc. Jpn.* **2013**, *82*, SA003.
- Triolo, A.; Russina, O.; Arrighi, V.; Juranyi, F.; Janssen, S.; Gordon, C. M. *J. Chem. Phys.* **2003**, *119*, 8549–8557.
- Yamamuro, O.; Inamura, Y.; Hayashi, S.; Hamaguchi, H. *AIP Conf. Proc.* **2006**, *832*, 73–80.
- Russina, O.; Beiner, M.; Pappas, C.; Russina, M.; Arrighi, V.; Unruh, T.; Mullan, C. L.; Hardacre, C.; Triolo, A. *J. Phys. Chem. B* **2009**, *113*, 8469–8474.
- Mamontov, E.; Luo, H.; Dai, S. *J. Phys. Chem. B* **2009**, *113*, 159–169.
- Aoun, B.; González, M. A.; Ollivier, J.; Russina, M.; Izaola, Z.; Price, D. L.; Saboungi, M.-L. *J. Phys. Chem. Lett.* **2010**, *1*, 2503–2507.
- Mamontov, E.; Baker, G. A.; Luo, H.; Dai, S. *Eur. J. Chem. Phys. Phys. Chem.* **2011**, *12*, 944–950.
- Yamamuro, O.; Yamada, T.; Kofu, M.; Nakakoshi, M.; Nagao, M. *J. Chem. Phys.* **2011**, *135*, 054508.
- Chathoth, S. M.; Mamontov, E.; Dai, S.; Wang, X.; Fulvio, P. F.; Wesolowski, D. J. *Europhys. Lett.* **2012**, *97*, 66004.
- Embs, J. P.; Burankova, T.; Reichert, E.; Hempelmann, R. *J. Phys. Chem. B* **2012**, *116*, 13265–13271.
- Chathoth, S. M.; Mamontov, E.; Fulvio, P. F.; Wang, X.; Baker, G. A.; Dai, S.; Wesolowski, D. J. *Europhys. Lett.* **2013**, *102*, 16004.
- Kofu, M.; Nagao, M.; Ueki, T.; Kitazawa, Y.; Nakamura, Y.; Sawamura, S.; Watanabe, M.; Yamamuro, O. *J. Phys. Chem. B* **2013**, *117*, 2773–2781.
- Burankova, T.; Reichert, E.; Fossog, V.; Hempelmann, R.; Embs, J. P. *J. Mol. Liq.* **2014**, *192*, 199–207.
- Kirchner, B., Ed. *Ionic Liquids*; Springer: New York, 2010; Vol. 290.
- Plechkova, N. V.; Seddon, K. R. *Chem. Soc. Rev.* **2008**, *37*, 123–150.
- Ohno, H., Ed. *Electrochemical Aspects of Ionic Liquids*, 2nd ed.; John Wiley & Sons, Inc.: Hoboken, NJ, 2011.
- Habasak, J.; Ngai, K. L. *The J. Chem. Phys.* **2008**, *129*, 194501.
- Turton, D. A.; Hunger, J.; Stoppa, A.; Hefter, G.; Thoman, A.; Walther, M.; Buchner, R.; Wynne, K. *J. Am. Chem. Soc.* **2009**, *131*, 11140–11146.
- Weingärtner, H. *Curr. Opin. Colloid Interface Sci.* **2013**, *18*, 183–189.
- Aoun, B.; González, M. A.; Russina, M.; Price, D. L.; Saboungi, M.-L. *J. Phys. Soc. Jpn.* **2013**, *82*, SA002.
- Kashyap, H. K.; Santos, C. S.; Annappureddy, H. V. R.; Murthy, N. S.; Margulis, C. J.; Castner, E. W. *Faraday Discuss.* **2012**, *154*, 133–143.
- Castner, E. W., Jr.; Margulis, C. J.; Maroncelli, M.; Wishart, J. F. *Annu. Rev. Phys. Chem.* **2011**, *62*, 85–105.
- Russina, O.; Triolo, A.; Gontrani, L.; Caminiti, R. *J. Phys. Chem. Lett.* **2012**, *3*, 27–33.
- Shimizu, K.; Bernardes, C. E. S.; Canongia Lopes, J. N. *J. Phys. Chem. B* **2013**, *118*, 567–576.
- Annappureddy, H. V. R.; Kashyap, H. K.; Biase, P. M. D.; Margulis, C. J. *J. Phys. Chem. B* **2010**, *114*, 16838–16846.
- Xiao, D.; Hines, L. G.; Li, S.; Bartsch, R. A.; Quitevis, E. L.; Russina, O.; Triolo, A. *J. Phys. Chem. B* **2009**, *113*, 6426–6433.
- Russina, O.; Triolo, A. *Faraday Discuss.* **2012**, *154*, 97–109.
- Faraone, A.; Hong, K.; Kneller, L. R.; Ohl, M.; Copley, J. R. D. *J. Chem. Phys.* **2012**, *136*, 104502.
- Stewart, J. R.; Deen, P. P.; Andersen, K. H.; Schober, H.; Barthélémy, J.-F.; Hillier, J. M.; Murani, A. P.; Hayes, T.; Lindenau, B. *J. Appl. Crystallogr.* **2009**, *42*, 69–84.
- D7—Diffuse Scattering Spectrometer; Institut Laue-Langevin: Grenoble, France, 2013; <http://www.ill.eu/?id=13310>.
- Tsuzuki, S.; Shinoda, W.; Saito, H.; Mikami, M.; Tokuda, H.; Watanabe, M. *J. Phys. Chem. B* **2009**, *113*, 10641–10649.
- See ref 35 and its associated Supporting Information.
- Moon, R. M.; Riste, T.; Koehler, W. C. *Phys. Rev.* **1969**, *181*, 920–931.
- Schärfp, O. *The Spin of the Neutron As a Measuring Probe*; O.Schärfp: München, Germany, 2010; host-82-135-31-182.customer.m-online.net/neutronpol.pdf.
- Richard, D.; Ferrand, M.; Kearley, G. J.; Bradley, A. D. *The Lamp Book*; Institut Laue-Langevin: Grenoble, France, 2013; <http://www.ill.eu/?id=2024>.
- Azuah, R. T.; Kneller, L. R.; Qiu, Y.; Tregenna-Piggott, P. L. W.; Brown, C. M.; Copley, J. R. D.; Dimeo, R. M. *J. Res. Nat. Inst. Stand. Technol.* **2009**, *114*, 341–358.
- Markwardt, C. B. *Astron. Data Anal. Software Syst. XVIII* **2009**, *411*, 251–254.
- Imanari, M.; Uchida, K.; Miyano, K.; Seki, H.; Nishikawa, K. *Phys. Chem. Chem. Phys.* **2010**, *12*, 2959–2967.
- See ref 2, pp 316–319.
- Unruh, T.; Smuda, C.; Busch, S.; Neuhaus, J.; Petry, W. *J. Chem. Phys.* **2008**, *129*, 121106.
- Stadler, A. M.; van Eijck, L.; Demmel, F.; Artmann, G. *J. R. Soc. Interface* **2011**, *8*, 590–600.
- Mitra, S.; Sharma, V. K.; Sakai, V. G.; Embs, J. P.; Mukhopadhyay, R. *J. Phys. Chem. B* **2011**, *115*, 9732–9738.
- Singwi, K. S.; Sjölander, A. *Phys. Rev.* **1960**, *119*, 863–871.
- Kneller, G. R. *Phys. Chem. Chem. Phys.* **2005**, *7*, 2641–2655.
- Volino, F.; Perrin, J.-C.; Lyonnard, S. *J. Phys. Chem. B* **2006**, *110*, 11217–11223.
- Sköld, K. *Phys. Rev. Lett.* **1967**, *19*, 1023–1025.
- Novikov, V. N.; Schweizer, K. S.; Sokolov, A. P. *J. Chem. Phys.* **2013**, *138*, 164508.
- Neumann, D. A.; Copley, J. R. D.; Cappelletti, R. L.; Kamitakahara, W. A.; Lindstrom, R. M.; Creagan, K. M.; Cox, D. M.; Romanow, W. J.; Coustel, N.; McCauley, J. P.; Maliszewskyj, N. C.; Fischer, J. E.; Smith, A. B. *Phys. Rev. Lett.* **1991**, *67*, 3808–3811.
- Sköld, K.; Rowe, J. M.; Ostrowski, G.; Randolph, P. D. *Phys. Rev. A* **1972**, *6*, 1107–1131.
- Cook, J. C.; Richter, D.; Scharpf, O.; Benham, M. J.; Ross, D. K.; Hempelmann, R.; Anderson, I. S.; Sinha, S. K. *J. Phys.: Condens. Matter* **1990**, *2*, 79–94.
- Vineyard, G. H. *Phys. Rev.* **1958**, *110*, 999–1010.
- Lovesey, S. W. *Theory of Neutron Scattering from Condensed Matter*; International Series of Monographs on Physics 72; Oxford University Press: New York, 1986; p 270.
- Leitner, M.; Vogl, G. *J. Phys.: Condens. Matter* **2011**, *23*, 254206.



(58) Farago, B.; Arbe, A.; Colmenero, J.; Faust, R.; Buchenau, U.; Richter, D. *Phys. Rev. E* **2002**, *65*, 051803.